UCRL 3887

UNIVERSITY OF CALIFORNIA

Radiation Laboratory

TWO-WEEK LOAN COPY

This is a Library Circulating Copy which may be borrowed for two weeks. For a personal retention copy, call Tech. Info. Division, Ext. 5545

ANGULAR DISTRIBUTIONS FOR (p, p') (p, d), AND (α, α') REACTIONS IN LITHIUM 7 AT MEDIUM ENERGIES

BERKELEY, CALIFORNIA

DISCLAIMER

This document was prepared as an account of work sponsored by the United States Government. While this document is believed to contain correct information, neither the United States Government nor any agency thereof, nor the Regents of the University of California, nor any of their employees, makes any warranty, express or implied, or assumes any legal responsibility for the accuracy, completeness, or usefulness of any information, apparatus, product, or process disclosed, or represents that its use would not infringe privately owned rights. Reference herein to any specific commercial product, process, or service by its trade name, trademark, manufacturer, or otherwise, does not necessarily constitute or imply its endorsement, recommendation, or favoring by the United States Government or any agency thereof, or the Regents of the University of California. The views and opinions of authors expressed herein do not necessarily state or reflect those of the United States Government or any agency thereof or the Regents of the University of California.

UCRL-3887
Physics and Mathematics

UNIVERSITY OF CALIFORNIA
Radiation Laboratory
Berkeley, California

Contract No. W-7405-eng-48

ANGULAR DISTRIBUTIONS FOR (p, p'), (p, d), AND (α, α') REACTIONS IN LITHIUM-7 AT MEDIUM ENERGIES

Robert Silver

(Thesis)

August 2, 1957

Printed for the U.S. Atomic Energy Commission

ANGULAR DISTRIBUTIONS FOR (p, p'), (p, d), AND (α, α') REACTIONS IN LITHIUM-7 AT MEDIUM ENERGIES

Contents

Abstract 4

Introduction

A. Inelastic Scattering 5

B. The Pickup Process 7

Experimental Apparatus

A. Proton Experiment 8

1. Beam Energy and Definition 8
2. Scattering Chamber 8
3. Targets 10
4. Detectors 10
5. Electronics 11
6. Beam Monitor 13

B. Alpha-Particle Experiment 13

1. The Beam and Scattering Chamber 13
2. Targets 15
3. Detectors and Electronics 15
4. Beam Monitor 16

Reduction of Data

A. Particle Identification 17

1. Alpha-Particle Experiment 17
2. Proton Experiment 18

B. Calibration of Detectors 22

1. Proton Experiment 22
2. Alpha-Particle Experiment 24

C. Target Thickness and Contaminants 24

1. Thickness Measurements 25
2. Contaminants 25

D. Kinematics 27

E. The Differential Cross Section 28

Errors 30

Results and Conclusions

A. Pulse-Height Spectra and Energy Levels in Lithium 32

1. Proton Experiment 32

2. Alpha-Particle Experiment 35
B. Angular Distributions 35
1. Inelastic Scattering 35
Appendix 46
A. 46
B. 48
Acknowledgments 49

ANGULAR DISTRIBUTIONS FOR (p, p'), (p, d), AND (α, α') REACTIONS IN LITHIUM-7 AT MEDIUM ENERGIES

Robert Silver

Radiation Laboratory
University of California
Berkeley, California

August 1, 1957

ABSTRACT

A natural lithium target has been bombarded by 31.8-Mev protons and the energy spectrum of the emitted particles taken every 10° from 10° to 120° and at 140° and 160°. Proton peaks corresponding to the ground state and to the 4.61-Mev, 6.6-Mev, and 9.6-Mev levels of Li^7 have been observed. Angular distributions for the 4.61- and 6.6-Mev levels of Li^7 have been obtained and fitted with the direct-interaction theory of Austern, Butler, and McManus. (Deuterons from the Li^6 ground state, 2.19-Mev, and 3.57-Mev levels have also been identified.) The ground-state and 2.19-Mev deuteron angular distributions have been fitted with the Butler pickup theory. In addition, lithium has been bombarded with 47.1-Mev alpha particles and an angular distribution obtained for the inelastically scattered alpha particles leaving Li^7 in the 4.61-Mev state. This distribution has also been fitted with the direct-interaction theory. Possible spins and parities have been assigned the levels for which angular distributions have been obtained.

INTRODUCTION

A. Inelastic Scattering

An increasing amount of evidence in recent years has pointed to the general validity of the proposal that the inelastic scattering process in the 10-to-50-Mev energy range can proceed through a direct type of interaction.[1] These reactions are direct in the sense that the formation of a compound state is not involved, and the reaction time is on the order of the transit time of the incident particle across the nucleus.

Previous descriptions had essentially been in terms of the formation and decay of a compound nucleus, where one considers the incident particle as having a short mean free path in nuclear matter and being quickly absorbed by the nucleus.[2,3] The energy of the incident particle is shared with the other nucleons and the compound nuclear state formed has a long lifetime compared with the transit time of a nucleon across the nucleus. Decay can take place only when enough energy is concentrated on one of the nucleons or groups of nucleons for it to penetrate through the nuclear surface.

The direct interaction as proposed by Austern, Butler, and McManus* is assumed to take place at the surface of the nucleus between the incident particle and one of the surface nucleons.[4,5] Contributions to the direct process from the rest of the nucleus are considered negligible. The validity of these assumptions requires that particles striking the nuclear core be absorbed into a compound state.

Although the yield of particles from the compound state may not be small compared with the yield from the scattering at the surface of the nucleus, one would nevertheless expect most of the former to have low energies, corresponding to high excitations of the residual nucleus, while the latter would favor the low excitation states of the residual nucleus. This suggests that the information obtained from the excitation of discrete low-lying states would best test the validity of the direct-interaction theory.

---

*Hereinafter referred to as ABM

The differential cross section obtained from the direct-interaction theory has the form of a diffraction pattern. The first maximum appears as a prominent peak at forward angles. The peak at forward angles can be considered a consequence of the fact that the center-of-mass system for the target nucleus and incident particle is not very different from the laboratory system for the incident particle and the single nucleon with which it interacts. This would result in a peak in the forward direction, but when angular-momentum restrictions are considered a peak at forward angles is still predicted although it need not occur at 0°.[6] The reaction products from the compound nucleus, on the other hand, are not expected to show the same degree of preference for the forward direction.

Distributions have been obtained by a number of investigators for the inelastic scattering of protons and alpha particles leading to discrete states.[1,5,7-14] The qualitative feature of a prominent forward peak has been obtained in most cases, although the results for the proton scattering off light nuclei near 10 Mev exhibit this effect to only a smaller extent.[7,8,12] The fitting of the forward peak with the ABM theory leads to the assignment of possible changes in the nuclear spin and to a determination of whether the parity of the final state is the same as or different from that of the initial state.

Other more complex models for the direct-interaction process have been proposed. The Bohr-Mottelson collective model considers the excitation of surface waves by the incident particle.[15] This leads to a similar type of expression for the angular distribution as obtained by ABM.

Hayakawa and Yoshida have extended the Bohr-Mottleson calculations to include the core effects.[16] These calculations are considerably more complicated, and no attempt has been made to carry out such calculations for the present data.

The investigation of the low-lying levels of Li^7 by the inelastic scattering of 31.8-Mev protons and 47.1-Mev alpha particles was undertaken because of the fundamental interest in this relatively simple nucleus and because little has been definitely established about the properties of its levels.[17]

B. The Pickup Process

In addition to the protons inelastically scattered from Li^7, deuteron groups corresponding to excited states of Li^6 can be expected from the proton bombardments. The production of deuterons at these energies is expected to proceed by the Butler pickup process.[18, 5]

This process and its inverse, the stripping reaction, are types of direct-interaction processes, and yield angular distributions similar to those for inelastic scattering by direct interaction. Considered from the standpoint of the specific reaction (p,α), the incoming proton is assumed to interact only with a neutron at the surface of the target nucleus without being affected by the rest of the nucleus. The proton and neutron then continue out of the nuclear surface as a deuteron.

That this simple picture is a good approximation for the first maximum is evidenced by the many data that have been fitted with the pickup and stripping theories.[19] Tobocman and Kalos have extended these calculations to include core interactions with the incident particle, and their results show that these effects can not always be ignored.[20]

EXPERIMENTAL APPARATUS

A. Proton Experiment

1. Beam Energy and Definition

The proton bombardments were carried out using the 31.8-Mev beam of the Berkeley proton linear accelerator.[21] The beam has an energy spread of about 100 kev and is approximately 1/4 inch in diameter. The actual beam energy may vary by as much as 0.5 Mev from day to day, although changes of the order of 0.1 Mev are more usual. The energy was measured by determining the ionization curve for the protons, using a variable aluminum absorber in front of an ionization chamber. The range in aluminum was taken as the value at 0.8 of the maximum of the ionization curve,[22] and the tables of Aron et al. were used to convert to energy.[23]

The beam-defining system is shown in Fig. 1. Here C_1, C_2, and C_3 are carbon collimators. C_1 is a remotely controlled 4-jaw collimator whose vertical jaws were set for 1/8 inch and whose horizontal jaws were used to control the beam intensity. The magnet serves as a switching device to steer the beam into the desired direction. C_2 is a 4-jaw adjustable collimator set with a 1/8-inch-square aperture. C_3 is a 3-foot triple collimator with the first aperture 1/8 inch in diameter (the main beam-shaping collimator) followed by 5/32-inch and 3/16-inch apertures 1 foot apart. The latter two apertures act to reduce the number of slit-scattered protons that enter the scattering chamber.

After collimation, the beam at the target is approximately 3/16 inch in diameter and has a maximum time-average intensity of about 4×10^{-9} ampere.

2. Scattering Chamber

The scattering chamber is 24 inches in diameter and has a remotely operated table that can be positioned in angle to $\pm 0.1^{\circ}$. A target changer that can hold up to six targets is attached to the lid. The selection of the target and the setting of its angle are also remote operations.

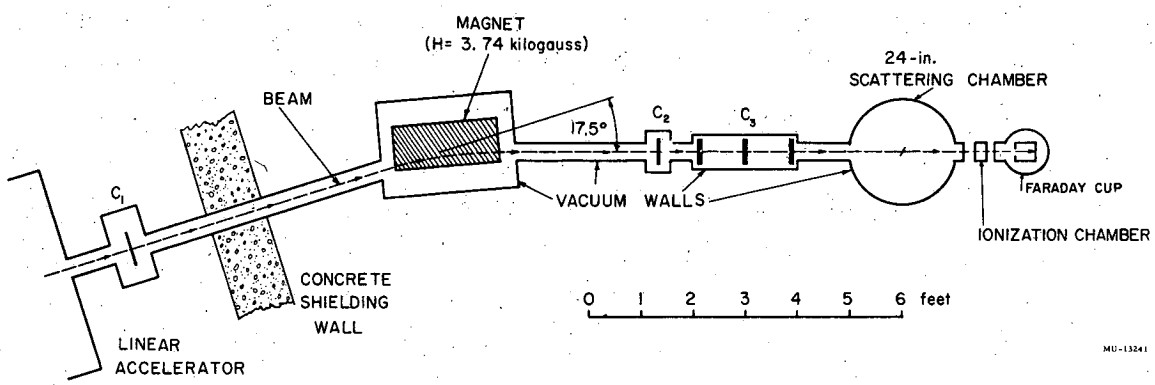

Fig. 1. Proton beam steering and collimation.

The remote indicator for the target angle was not operating, however, and the target angle was set by using a scale on the target changer. This could be read to $\pm 0.5^{\circ}$.

Alignment of the chamber and collimators along the beam line was done optically. The beam line was determined by the fixed collimator, C_2, and by a spot burned in a glass plate by the beam at the exit end of the scattering chamber.

3. Targets

The targets used were of the order of 0.005 inch thick. They were prepared from natural lithium by rolling freshly cut slices of lithium to the desired thickness in a dry box containing an argon atmosphere. The targets were placed on a holder and enclosed in a plastic envelope while still in the dry box. This permitted removal of the targets to the scattering chamber and their attachment to the target changer without exposure to air. After the chamber was evacuated the envelope around the target was removed mechanically by raising the target holder up into the target chamber. A gate valve between the target chamber and scattering chamber allowed the target to be isolated in the target-chamber vacuum whenever it was necessary to open the scattering chamber.

4. Detectors

Two separate scintillation counters were used. One was a NaI(Tl) crystal and photomultiplier tube, and the other a plastic scintillator and photomultiplier tube. The photomultipliers were DuMont 6291 tubes operated at reduced voltages (700 to 800v) to prevent saturation in their outputs. They were selected for low noise output and good pulse-height resolution. Both detectors were mounted in the scattering chamber with a vacuum fitting such that the entire crystal photomultiplier tube assembly was at atmospheric pressure, thus avoiding the Geissler discharge region while the chamber was being pumped down.

a. The NaI(Tl) counter

The NaI(Tl) crystal was prepared in a dry box containing a nitrogen atmosphere. The crystal was cleaved and rough sanded to 7/8 by 7/8 by 5/16 inch. The 5/16-inch dimension was chosen

to be more than the range of a 32-Mev proton in order to allow for subsequent refinishing of the crystal. The crystal was mounted in a lucite holder to which a 0.0005-inch aluminum window was attached. The inner surfaces of the holder were painted with Tygon white paint for high reflectivity, except for the polished side in contact with the photomultiplier tube. Dow-Corning silicone grease (10^6 cs) was used in the interface between the crystal and lucite and the lucite and photomultiplier in order to optimize the optical coupling.

The energy resolution as determined from the elastic peak (full width at one-half maximum) varied from 2.6% at forward angles to 4.5% at backward angles. Computing the contributions to the resolution due to the target, the beam width, the angular aperture of the counter, and the channel widths of the analyzer shows that the resolution of the NaI crystal and photomultiplier tube alone is 2.5% at best. The poor resolution at backward angles is probably caused by these angles having been run at the end of the experiment, at which time the crystal surface gave evidence of being contaminated.

b. The plastic scintillation counter

The plastic scintillator was a 5/8-inch cube of terphenyl-loaded polystyrene. The optical path to the photomultiplier tube was through a short light pipe. Silicone grease was used to insure good optical contact at both ends of the pipe. To improve the light-collecting efficiency the scintillator was covered with an aluminum foil hood.

The counter was used to take data in the angular interval from 10° to 90°, and the energy resolution, taken from the elastic peak, was on the order of 4.5% for the whole interval.

5. Electronics

Figure 2 is a block diagram of the electronics. Separate high-voltage supplies were used to maintain independent and continuous operation of the two counters. The hv supplies were regulated to better than 0.02%. The signal from each photomultiplier tube was fed into separate cathode

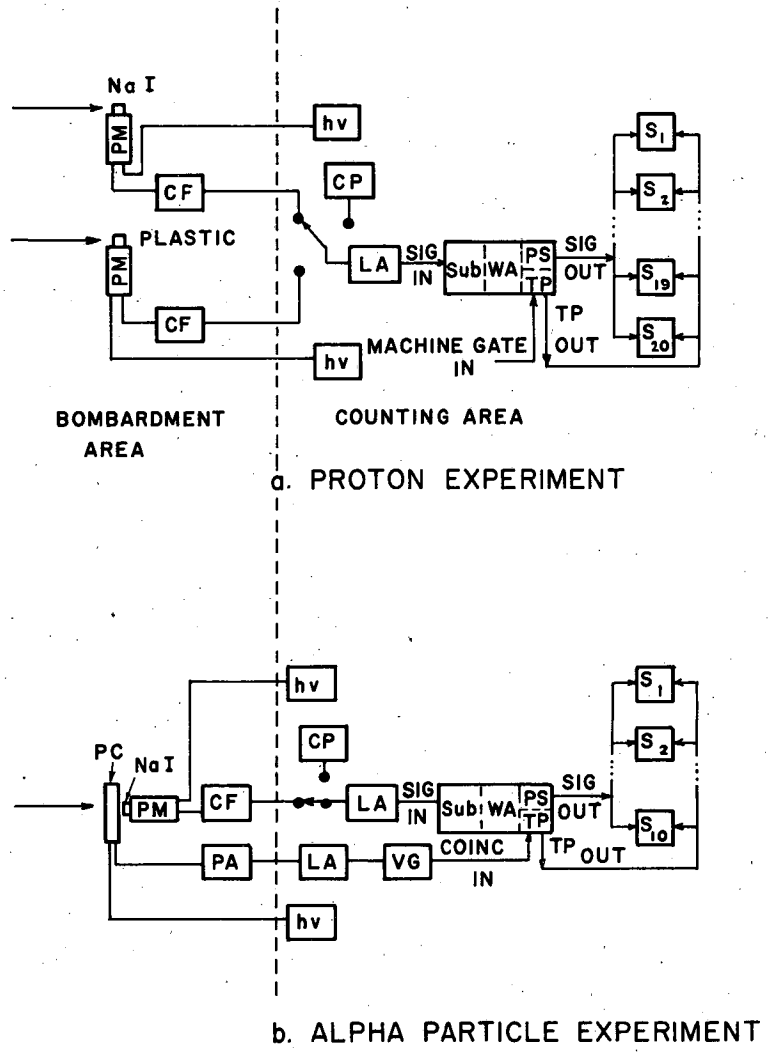

MU-13994

Fig. 2. Electronics block diagrams.

PM - Photomultiplier	CP - Calibration pulser
PC - Proportional counter	Sub - Voltage subtractor
CF - Cathode follower	WA - Window amplifier
PA - Preamplifier	PS - Pulse stretcher
LA - Linear amplifier	PT - Timing-pulse generator
VG - Variable gate	
hν - High-voltage supply	S - Scalers

followers whose input time constants were chosen to give 1.5-μsec output pulses. Data were taken with only one counter at a time so that the output of either cathode follower was fed into a linear amplifier and then into the pulse-height analyzer.

The analyzer consisted of a chassis containing a voltage subtractor, an amplifier, a pulse stretcher, and a timing-pulse generator, followed by a bank of scalers whose inputs had been modified.[24] The modification consisted of a coincidence and anticoincidence network arranged so that the signal would record only in the scaler representing the proper pulse-height interval. With the resolution attainable from the NaI(Tl) crystal it was desirable to operate the analyzer with 1-volt channel widths (~0.5 Mev per volt). Stability with such narrow channels required temperature control of the window-amplifier chassis, the linear amplifier, and the calibration pulser (used to set the channel widths). The proton data were taken with the analyzer extended from its usual 10-channel operation to 20 channels.

6. Beam Monitor

After passing through the target and an exit window in the scattering chamber, the beam was collected in a Faraday cup and the resulting voltage across a capacitor (known to 0.1%) was measured by a 100%-feedback electrometer. The voltage was recorded on a Leeds and Northrup recording millivoltmeter. Permanent magnets were used at the entrance to the cup to prevent the escape of secondary emitted electrons. An ionization chamber in front of the Faraday cup served as the beam monitor for the linear accelerator crew.

B. Alpha-Particle Experiment

1. The Beam and Scattering Chamber

The 60-inch Crocker Laboratory cyclotron was used for the alpha-particle bombardments. The beam was brought out of the cyclotron by a procedure described by Ellis,[25] and directed into a 36-inch scattering chamber (see Fig. 3). The scattering chamber has the same features as

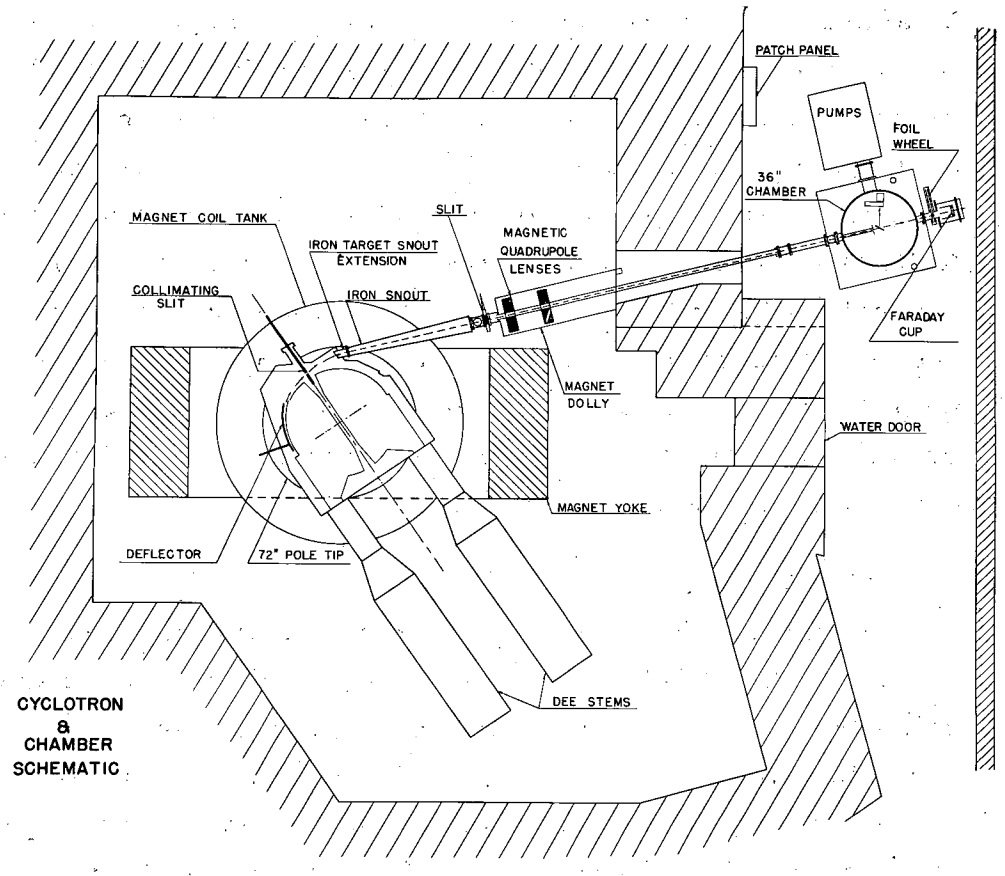

Fig. 3. Diagram of the alpha-particle experimental arrangement.

the 24-inch chamber previously described in this paper. By means of a quadrupole focusing magnet and a carbon collimation system, a 1/8-inch-diameter beam was passed through the target at the center of the scattering chamber. The beam-shaping aperture of the collimating system was 1/8 inch in diameter. It was followed by a 3/8-inch aperture, 6 inches away, to eliminate slit-scattered alpha particles. The collimators and the scattering chamber were optically aligned along the beam path.

The mean beam energy as determined from number-range curves in aluminum was 47.1 ± 0.5 Mev.

2. Targets

The targets, as in the proton experiment, were about 0.005 inch thick, and were made and transferred to the scattering chamber by the same technique as outlined in that section.

3. Detectors and Electronics

The data counter was a NaI(Tl) crystal mounted on the face of a DuMont 6292 photomultiplier tube. A proportional counter in front of the crystal was used to discriminate between alpha particles and less heavily ionizing particles. This counter has been fully described by Fischer.[7]

The output of the proportional counter, after passing through a preamplifier and a linear amplifier, went into a variable gate unit. (See Fig. 2.) The variable gate output was then fed into the pulse-height analyzer where it formed a coincidence with the NaI counter signal. The discriminator of the variable gate was set to count all the elastically scattered alpha particles at the smallest angle for which data were taken. This setting prevented the recording of particles other than alpha particles in the pulse-height intervals investigated.

The remaining electronics was identical to that used in the proton experiment except that the analyzer had only 10 channels.

4. Beam Monitor

Integration of the beam was by means of a Faraday cup and electrometer. As an additional beam monitor a NaI(Tl) counter was placed in a fixed position outside a window of the scattering chamber. It counted the particles scattered from the target at about 18°. The crystal monitor was calibrated against the Faraday cup and used as the beam integrator for small angles ($\leq 11^{\circ}$) when part of the beam struck the shielding of the data counter. It also acted as a monitor for the cyclotron crew.

REDUCTION OF DATA

A. Particle Identification

In both experiments it was desirable to use a particle-detection and analyzer system that permitted the recording at one time of as large a segment of each energy spectrum as possible. In this way the spectra and cross sections obtained from them would not be very sensitive to shifts in the beam energy. The use of a scintillation counter and multichannel analyzer appeared to be the logical choice.

With a single scintillation counter some information can be obtained on the identity of particle groups contributing to the energy spectra. In particular, proton and deuteron groups from a light nucleus show a strong differential energy shift as the angle of observation is changed; by this property alone the identities of different groups may be determined. A differential energy shift with changing angle is also observed for two groups of the same detected particle if the recoil particles are very different in mass. This technique, of course, requires that the counter be calibrated in energy, at least approximately, for the various particles, and that the reactions be known, in order to calculate their kinematics.

This method was employed in both experiments wherever possible. It permitted the identification of enough deuteron groups in the proton experiment to get a good calibration for the plastic scintillator (see Calibration of Detectors). In the alpha-particle experiment it was very useful in distinguishing between the alpha-particle groups scattered from Li^7 and those scattered from the hydrogen contaminant in the target. Nevertheless a more positive means of particle identification was needed.

1. Alpha-Particle Experiment

Protons, deuterons, and tritons could appear in the alpha-particle spectra either as discrete groups or as part of the continuum near the peak corresponding to the 4.61-Mev level of Li^7. It was a relatively easy matter to discriminate against them by means of their dE/dx,

measured with a proportional counter placed before the NaI detector. It was possible to set the discriminator of the variable-gate unit at a single setting for all the data (see Fig. 2 for electronics diagram). This setting was selected to discriminate against pulses smaller than those from the elastically scattered alpha particles at the smallest angle of observation (6°). This insured that alpha particles from angles equal to or greater than 6° would produce pulses in the proportional counter large enough to trigger the discriminator circuit and gate the analyzer "on."

Calculations were made to check the effectiveness of this setting against protons, deuterons, tritons and He^3 particles. Protons, deuterons, or tritons with enough energy to record in the pulse-height analyzer would not give a big enough pulse in the proportional counter to gate the analyzer "on." A He^3 particle could gate on the analyzer, but the Q for the reaction $Li^7(\alpha, He^3)Li^8$ (Q=-18.5 Mev) fortuitously restricts the possible energies for the He^3 to below the analyzer threshold.

Runs with and without the proportional counter showed a decrease of 10% to 20% in the continuum under the 4.61-Mev peak, but did not show the presence of any peaks due to particles lighter than alphas.

2. Proton Experiment

In the proton experiment, in which it was desired to detect protons, deuterons and, if possible, tritons and alpha particles, the use of the proportional counter—scintillation counter combination with a multi-channel pulse-height analyzer presented a more difficult problem. The use of such a system with the 20 channels needed to get the data in a reasonable period of time would have made the electronics considerably more complicated, with a corresponding increase in maintenance problems.

It was felt that the additional information about the detected particles needed to identify them could be provided more simply by using a second detection system that responded differently to the particles than did the first. A NaI(Tl) crystal counter was constructed as the primary detector to take advantage of its better energy resolution as compared with other scintillating materials. For the second counter a plastic scintillator was chosen. The response of these materials to protons and deuterons is shown in Fig. 4.

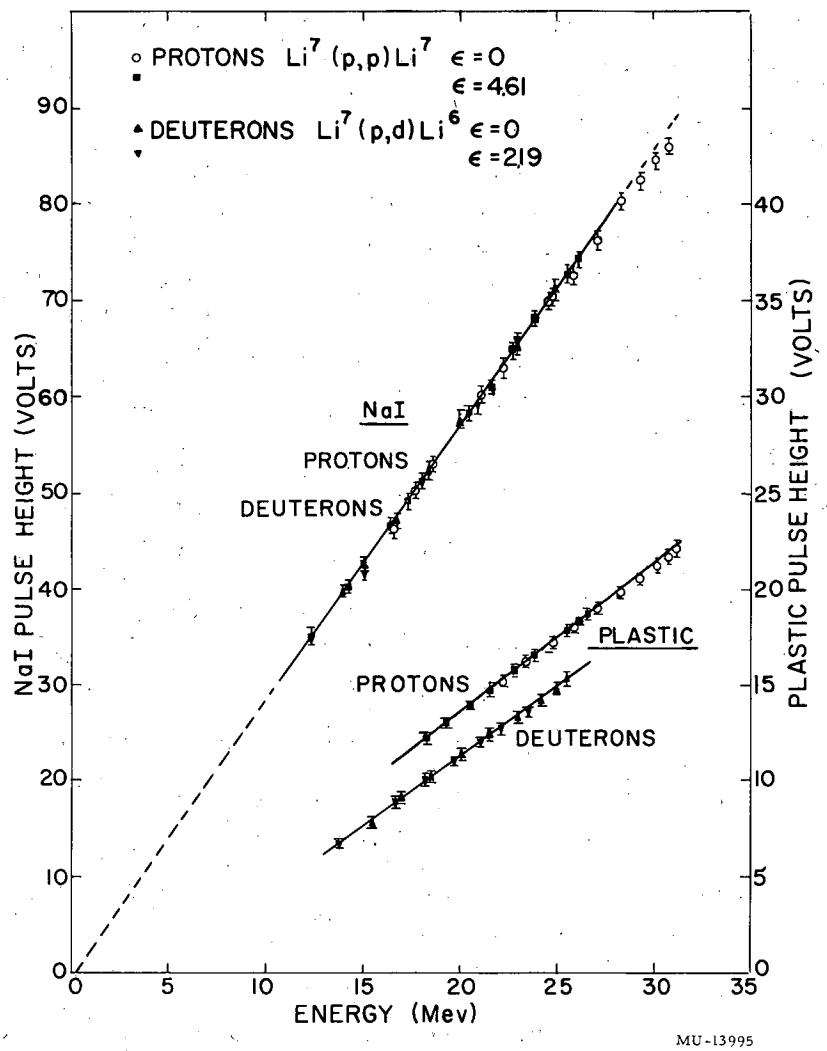

Fig. 4. Responses of sodium iodide and plastic scintillator crystals to protons and deuterons.

Both counters were used to obtain spectra at each angle, with approximately half of the data being taken with each. Figure 5 shows portions of such spectra taken at 20^{o}(lab). The diagonal lines represent the pulse-height—versus—energy calibration of the detectors for protons and deuterons.

Peaks A coresspond to the protons elastically scattered from Li^{7}. They appear at the same proton energy in both spectra--as they should, since they were used in the calibration of the detectors for protons. The higher and sharper peak in the NaI spectrum, as compared to the peak in the plastic spectrum, is a result of the better energy resolution of the NaI.

Peaks B are seen to have the same proton energy, and occur at the proper position for the 4.61-Mev level of Li^{7}.

Peaks C, when considered as deuterons, have the same energy, and correspond to $Li^{7}(p, d)Li^{6}$(ground state). Neither peak has a possible proton counterpart in the other spectrum.

Peak D of the NaI spectrum has no proton counterpart in the plastic spectrum, and has the correct deuteron energy for the 2.19-Mev level of Li^{6}. Its deuteron counterpart in the plastic spectrum occurs at the position D'. The broken line under D' indicates the general background level in that region of the spectrum. On the basis of an approximate calibration (see Calibration of Detectors), the high points to the left of D may be in part due to alpha particles or tritons from the reactions $Li^{7}(p, \alpha)He^{4}$ and $Li^{7}(p, t)Li^{5}$(ground state). Their positions in the NaI spectra would be at 63 volts and 52 volts, respectively. It should also be noted that the general structure on the low-energy side of D appears to have no proton counterpart in the plastic spectrum, and probably includes deuterons corresponding to the 3.57-Mev level of Li^{6}.

The hump on the high-energy side of B in the NaI spectrum corresponds to p-p scattering from the hydrogen contaminant in the target. Although the statistics are poor it appears to have a proton counterpart in the plastic spectrum. The small peak between B and C in the plastic spectrum corresponds to the 6.6-Mev level of Li^{7}.

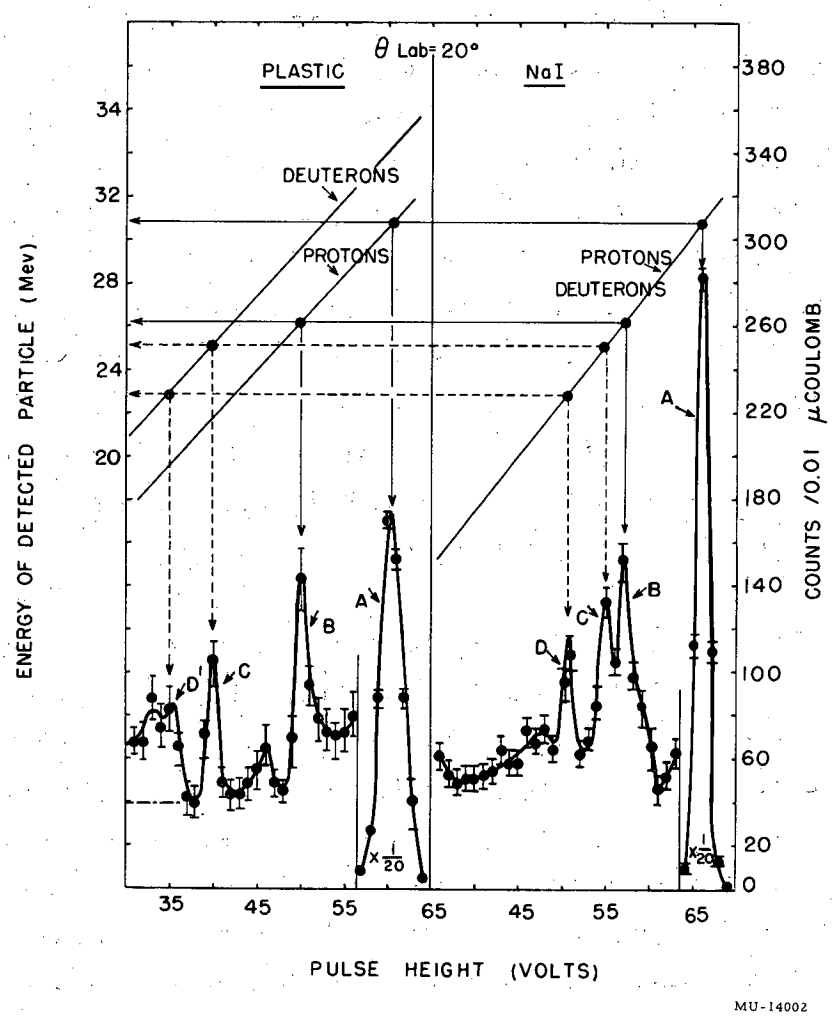

Fig. 5. Use of differential pulse-size response to identify particles.

B. Calibration of Detectors

1. Proton Experiment

The NaI and plastic scintillation detectors were calibrated for protons, using the protons elastically scattered from Li^7. Their energy as a function of angle was calculated from the kinematics and corrected for losses in the target and the detector foils. The response in the NaI was found to be linear in the region between 15 and 30 Mev (see Fig. 4). This is in agreement with the published data.[26, 27, 28] In addition, the linearity has been shown by Allison and Casson to extend down to a few kev.[27] Agreement is indicated in the results presented here by the fact that a linear extrapolation to zero pulse height passes the line through the origin, within experimental error. The response of the plastic was also found to be linear over approximately the same energy interval, and is in good agreement with the data of Hecht.[11] This curve, linearly extrapolated to zero pulse height, intercepts the energy axis at about 2.5 Mev. This is a consequence of the nonlinear response of plastic scintillators to proton energies below about 10 Mev.

The proton calibration of the NaI also served as a calibration for deuterons, since the response of NaI is the same for deuterons and protons.[26]

As a preliminary calibration for deuterons in the plastic scintillator, the published data on the organic scintillators, stilbene and anthracene, were used.[26, 28] As a class the organic scintillators, while having different efficiencies for conversion of energy to light, have similar responses to stopping particles. The response to protons obtained with the plastic scintillator in this experiment has the same shape as given for stilbene and anthracene crystals. It is reasonable to assume that these crystals respond about the same deuterons as do the plastic scintillator. As a check of this assumption the three points obtained by Hecht for deuterons of 10 to 14 Mev were put on this plot. Although the agreement was within statistics, it suggested that the energy separation between the two curves should be larger.

As the final calibration, additional deuteron points were obtained from the actual data by the following procedures:

(a) Peaks corresponding to particles other than protons could often be identified by comparing the NaI and plastic spectra at the same angle. Such peaks would shift their positions relative to the known proton peaks. C and D in Fig. 5 are examples of "nonproton" peaks.

(b) If it is assumed that the "nonproton" peaks are deuterons, their energies can be determined from the NaI calibration and the preliminary calibration of the plastic. From the kinematics the peaks that correspond to expected deuteron energies can then be selected.

(c) Next, the change in energy with angle for each tentatively identified deuteron peak can be compared with the kinematics. In this connection the peaks that would correspond to the ground state of Li^6 in the spectra from 60° to 90° (lab) were the most useful. This is because the kinematics eliminates the possibility of their being tritons; and alpha-particle peaks could easily be distinguished from deuteron peaks by their rate of change of energy with angle.

(d) Finally, the corresponding deuteron peaks in each pair of spectra can be found by comparing energies and cross sections.

Deuteron points in the energy interval from 15.5 to 20 Mev were obtained in this manner. They were in agreement with Hecht's points, and required the displacement of the preliminary deuteron curve an additional 0.5 Mev from the proton curve. The separation between protons and deuterons was 3 Mev in this energy region.

The final calibration of both detectors is shown in Fig. 4. Proton and deuteron points corresponding to the 4.61-Mev level of Li^7 and the 2.19-Mev level of Li^6, respectively, are also plotted.

It was also necessary to have some idea where triton and alpha-particle peaks might occur in the spectra. The tritons are produced in the reaction $Li^7(p, t)Li^5$ with $Q = -4.27$ Mev. The reaction $Li^7(p, \alpha)He^4$ with $Q = +17.34$ Mev is the source of the alpha particles. Their energies are high enough to place them in regions of the spectra being analyzed for protons and deuterons. For getting an idea of where to expect

them, the data of Taylor et al. were used to get approximate response curves for alphas in both detectors.[26] No data were available on tritons, therefore a reasonable estimate of the position of the triton curve was made. No peaks in either spectra could be established as caused by either tritons or alphas. Small but detectable peaks may have been present, but were not identified. Nevertheless, with the aid of the kinematics, the curves provided information on the regions of the spectra where tritons and alphas might produce trouble in the analysis.

2. Alpha-Particle Experiment

It was necessary to calibrate the NaI detector only for alpha particles, because the proportional counter was used to prevent the recording of other particles in the analyzer. In addition, an accurate calibration was not required because the peak corresponding to the 4.61-Mev level of Li^7 was readily identifiable at most angles. An adequate calibration was obtained by using the pulse heights of the elastic and 4.61-Mev peaks and the scattered alpha-particle energy calculated from the kinematics without correction for losses in the target and the detector foils.

C. Target Thickness and Contaminants

A single target was used for all the proton bombardments except for the data taken at 15°, 45°, and 75°. These data were normalized to the principal target data by means of the elastic cross sections.

Three different targets were used in the alpha-particle bombardments. The thickness of only the first was measured, and data taken at 13° were used to normalize the remaining data.

A target angle of 45° was used for all the data in both the proton and the alpha-particle experiments. Data were taken in the quadrants containing the normal to the target surface.

1. Thickness Measurements

In the alpha-particle experiment the target thickness was measured by taking number-vs-range curves for the incident alpha-particle beam, with and without the target in place. The difference in the mean ranges gave the target thickness in aluminum equivalent. This method measured $t/\cos\theta_t$, for which the value 5.86+0.29 mg/cm^2 was obtained.

The same technique was tried in the proton experiment but the results were not satisfactory because of beam-intensity fluctuations. The target was therefore removed from the scattering chamber with a minimum of exposure to air and returned to the dry box. A triangular section was cut from the center of the target. This was transported in a container with an argon atmosphere to an accurate balance. The weight of the triangle was recorded over a sufficiently long period of time to establish the rate of change in its weight when exposed to air. It was a linear function of time for the interval considered (approximately thirty minutes.) Then an extrapolation was made to obtain the weight at the time of removal from the chamber. The dimensions of the triangle were measured and the target thickness calculated. The thickness was 6.32+0.25 mg/cm^2. This includes the oxygen contamination present during the bombardments.

2. Contaminants

During the preparation of the targets some darkening of the surfaces occurred, but no further deterioration was noticeable once the target was placed in the vacuum of the scattering chamber.

In the proton experiment a check was made for contaminants by extending the energy spectra obtained at 60° and 70° to include protons with energies greater than that of the Li^7 elastic peak. These spectra showed the presence of oxygen as the main contaminant, with smaller amounts of carbon and sodium. Care was taken in analyzing the data to avoid confusing the levels of oxygen with a level in Li^7 having a small cross section. The amounts of sodium and carbon present were not large enough to require special precautions in the data analysis.

The amount of oxygen present was determined by using the differential elastic cross-section values of Kinsey and Stone for proton scattering

from oxygen at this energy.[29] The target was found to contain 5% of oxygen by weight. The target thickness corrected for the oxygen was 5.95 ± 0.26 mg/cm^2.

Another contaminant was hydrogen, indicating that the darkening of the surface was due to lithium hydroxide. This peak was small and predictable in position so that it could be located when the data were analyzed.

An alpha-particle group corresponding to elastic scattering from hydrogen also appeared in the energy spectra from the alpha-particle bombardments. No attempt was made to determine the other contaminants in these targets, although oxygen was very likely another contaminant.

D. Kinematics

For the calibration of the counters and assignment of excitation energies to the residual nuclei the kinematics for the reactions investigated in this experiment had to be known.

The two-body reaction in the laboratory system can be represented by

$$E_1 + M_1 + M_2 \rightarrow M_3 + M_4 + \epsilon + E_f ,$$

where

M_1 is the incident particle,

M_2 is the target nucleus,

M_3 is the detected particle,

M_4 is the residual nucleus,

E_1 is the kinetic energy of the incident particle,

ϵ is the excitation energy of the residual nucleus, and

E_f is the kinetic energy of the detected particle plus that of the residual nucleus.

The energy (nonrelativistic) of the detected particle (M_3) in the laboratory system is given by

$$E_3 = \frac{M_1 M_3}{(M_1 + M_2)^2} E_1 \left[\cos\theta \pm \sqrt{\frac{1}{r^2} - \sin^2\theta}\right]^2 ,$$

where

$$\frac{1}{r^2} = \left(\frac{V_3^*}{V_{c.m.}}\right)^2 \simeq \frac{M_2 M_4}{M_1 M_3} \left[1 + \frac{M_1 + M_2}{M_2} \frac{(Q-\epsilon)}{E_1}\right],$$

for $\dfrac{Q}{(M_3 + M_4)C^2} << 1$.

The remaining symbols defined as follows:

E_3 is the kinetic energy of the detected particle,

θ is the scattering angle of the detected particle in the laboratory system,

V^*_3 is the velocity of the detected particle in the center-of-mass system,

$V_{c.m.}$ is the velocity of the center of mass,

$$Q = \left[(M_1 + M_2) - (M_3 + M_4)\right] c^2 ,$$

c is the velocity of light.

In the expression for E_3, only the plus sign is used for reactions in which $\frac{1}{r^2} \geq 1$. For $\frac{1}{r^2} \leq 1$, E_3 is double-valued and both signs are needed.

For the proton experiment the energies were corrected for losses in the target and the counter foils. Plots of E_3 (corrected) vs θ and E_3 (corrected) vs ϵ for the observed reactions were used in the calibration of the counters and the assignment of excitation energies to the residual nuclei. The target and foil corrections were not made for the alpha-particle experiment, as the 4.61-Mev level could readily be identified by use of plots with E_3 uncorrected.

E. The Differential Cross Section

The differential cross section in the center-of-mass system is given by

$$\frac{d\sigma}{d\Omega} = \frac{N_s}{\Delta\Omega N_i n_t} \cdot G \frac{cm^2}{sterad} \quad (c.m.),$$

where N_s is the number of particles scattered into the solid angle $\Delta\Omega$,

$\Delta\Omega$ is the solid angle subtended by the counter aperture at the target,

N_i is the number of particles incident on the target,

n_t is the number of target nuclei per cm^2 along the beam direction (this includes only nuclei of the kind producing the observed reaction), and

$G \equiv \frac{d\Omega(lab)}{d\Omega(c.m.)}$ is the laboratory-to-center-of-mass transformation factor for the solid angle.

Writing N_i and n_t in terms of measured and known quantities, we have

$$N_i = \frac{CV}{e} \quad \text{and} \quad n_t = \frac{t\,N_o}{A \cos \theta_t},$$

where C is the capacitance in the beam-integrating circuit (in farads),

V is the electrometer potential (in volts),

e is the electronic charge (in coulombs),

t is the target thickness (in g/cm^2),

θ_t is the angle between the beam direction and the normal to the target surface,

A is the atomic weight of the target nuclei, and

N_o is Avogadro's number.

On substitution for N_i and n_t, the differential cross section becomes

$$\frac{d\sigma}{d\Omega} = \frac{N_s G \; e A \cos \theta_t}{C V \Delta\Omega N_o \; t} \; \frac{\text{cm}^2}{\text{sterad}} \quad \text{(c.m.)}$$

N_s is equal to $(\sum_j N_j)$-B, where N_j is the number of counts in the j th channel, and the summation is over the channels included between the minima on either side of the peak. B is the number of background counts under the peak and is determined by drawing a smooth curve between the minima. In the drawing of the background line an attempt is made to give it a reasonable shape based on observed trends as a function of angle. When the background level is uncertain, the range of possible background lines is considered, and this uncertainty is included in the error assigned the cross section.

The conversion factor G is given by

$$G \equiv \frac{d\Omega(\text{lab})}{d\Omega(\text{c.m.})} = \frac{(1 - r^2 \sin^2 \theta)^{1/2}}{\left[r \cos \theta + (1 - r^2 \sin^2 \theta)^{1/2}\right]^2},$$

where θ is the scattering angle in the laboratory system and r is defined in the section on Kinematics.

The laboratory angle, θ, transforms to the c.m. angle, ϕ, by $\sin(\phi - \theta) = r \sin \theta$.

ERRORS

The standard deviations plotted on the graphs are the errors in the relative cross sections only. They were obtained from the counting statistics and include an estimate of the error involved in the determination of the background line.

Because N_s and G are both functions of θ, the counter angle in the laboratory system, uncertainties in θ contribute to the errors in the relative cross sections. The error in N_s is greatest where $d(\ln N_s)/d\theta$ is a maximum; that is, at the point of maximum slope of the differential cross section on a semilogarithmic plot. For an uncertainty of $\pm 0.1^{\circ}$ in the counter angle we have

$$\frac{\delta N_s}{N_s} \leq 1\% \text{ for the proton angular distributions,}$$

$$\leq 1.5\% \text{ for the deuteron angular distributions,}$$

$$\leq 3\% \text{ for the alpha-particle angular distributions.}$$

The error in G can be neglected, as it is always $< 0.1\%$ for $\delta\theta = \pm 0.1^{\circ}$.

The remaining quantities contributing to the errors in the absolute cross sections are

$$\frac{\delta C}{C} = 0.1\%$$

$$\frac{\delta V}{V} = 0.5\% .$$ The only contribution to this quantity is from the recording of the potential. The loss of charge from the Faraday cup due to leakage and multiple Coulomb scattering in the target is negligible.

$$\frac{\delta(\Delta\Omega)}{\Delta\Omega} = 3.8\% \ (p, p') \text{ and } (p, d) \ .$$

$$= \quad 2\% \ (\alpha, \alpha')$$

$$\frac{\delta(\cos\theta_t)}{\cos\theta_t} = 0.9\% \quad \text{for } \delta\theta_t = 0.5^\circ \ .$$

$$\frac{\delta t}{t} = 4.4\% \ (p, p') \text{ and } (p, d) \ .$$

$$\frac{\delta\left(\frac{t}{\cos\theta_t}\right)}{\frac{t}{\cos\theta_t}} = 5.0\%^* \ (\alpha, \alpha') \ .$$

Where specific reactions are indicated after a quantity, the quantity refers only to those reactions.

The combined errors, not including counting statistics, are

6.0% for (p,p')
6.1% for (p, d) ,
6.2% for (α, α') .

These errors are to be combined with the relative errors given on the plots to give the error in the absolute cross sections.

---

*The quantity measured in the alpha experiment was $t/\cos\theta_t$, that is, the target thickness as seen by the beam. (See section on Target Thickness.

RESULTS AND CONCLUSIONS

A. Pulse-Height Spectra and Energy Levels in Lithium

1. Proton Experiment

Energy spectra were taken every 10° from 10° to 90° with both detectors. In addition the NaI detector was used to obtain spectra at 100°, 110°, 120°, 140°, and 160°. A typical spectrum is shown in Fig. 6.

Peaks corresponding to the ground-state and 4.61-Mev level of Li^7 were readily identified in all the spectra. For angles of 60° and less, data on the 6.6-Mev level of Li^7 were obtained from the plastic spectra. This was necessitated by the movement of the deuteron peaks corresponding to the Li^6 ground-state and 2.19-Mev level across the position of the 6.6-Mev peak in the NaI spectra.

Evidence for the excitation of Li^7 to the 9.6-Mev level was obtained from the plastic spectra at 50°, 60°, and 70° (see Fig. 7). At other angles it was not observed or could not be resolved from other peaks. The excitation of the 7.46-Mev level of Li^7 was uncertain. Its cross section is small, and where a peak does appear at the expected position of the 7.46-Mev level one cannot exclude the possibility that it might correspond to a level in Li^6 (7.5% isotopic abundance).

Levels of Li^6 observed by (p, d) reaction were the ground state, the 2.19-Mev level, and the 3.57-Mev level. The first two were seen in both spectra at angles below 90°. A positive identification of the 3.57-Mev level was made only at 30°. At angles of 90° and greater the deuteron peaks appeared displaced toward lower pulse heights. These data were taken last, and the displacement could have resulted from contamination of the front surface of the NaI crystal. No deuteron data were taken from these later spectra.

The sharp rise in the continuum at the threshold for the $Li^7(p, p')H^3He^4$ reaction (see Fig. 6) is characteristic of all of the spectra except at 10° and 20°, where it was obscured by the large elastic peak.

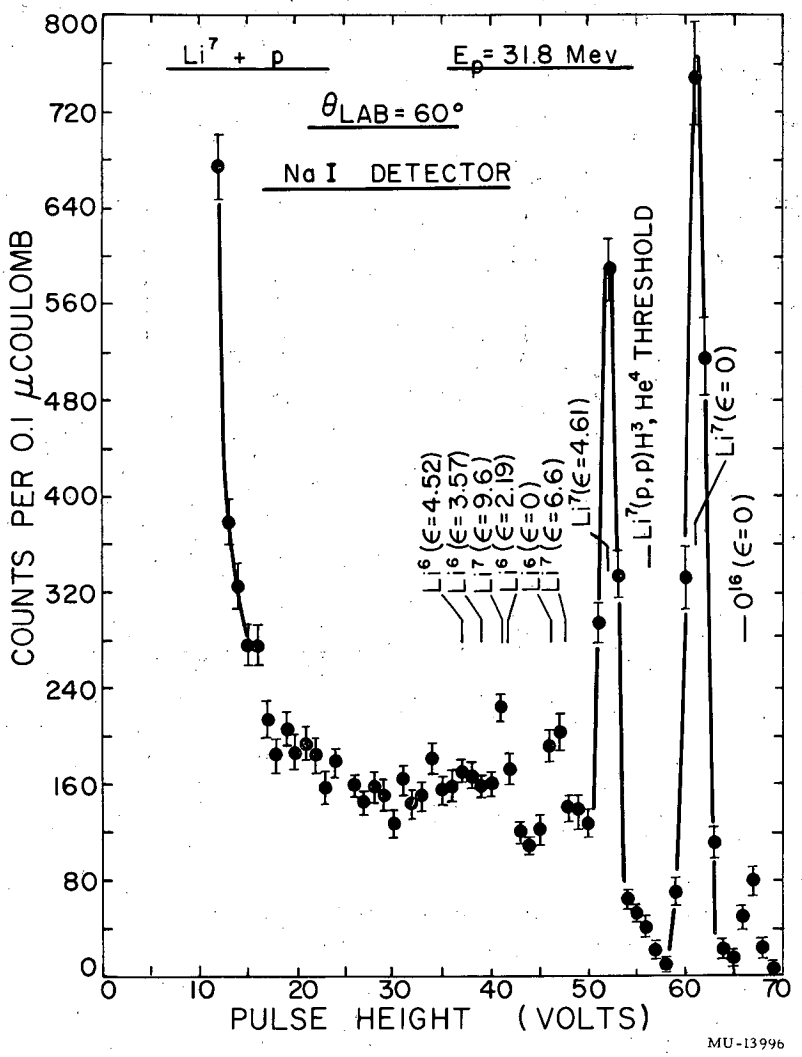

Fig. 6. Sodium iodide spectrum for 60° in the proton experiment.

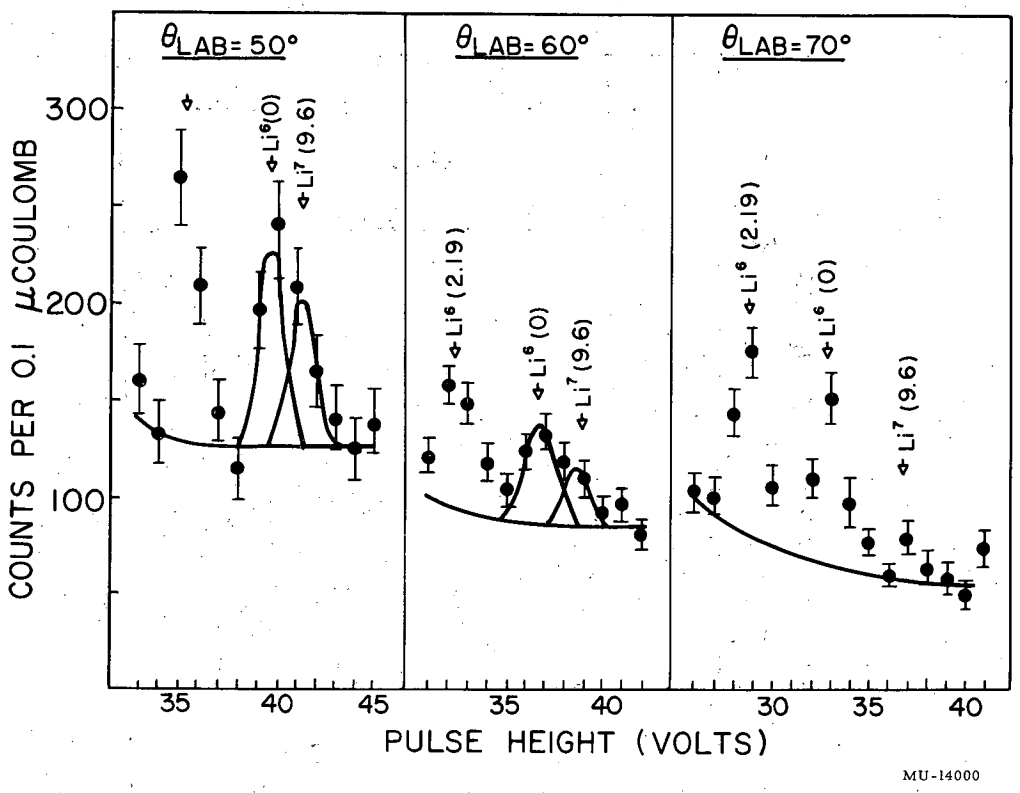

Fig. 7. Appearance of the 9.6-Mev level of Li^7 in the proton experiment.

2. Alpha-Particle Experiment

Observations of the scattered alpha particles were taken only for that portion of the spectrum near the 4.61-Mev peak. Data were taken in approximately 1° intervals from 6° to 20° and every 5° thereafter to 65°. Figure 8 shows the spectrum obtained at 13°. The continuum under the peak is due to the three-body breakup, $Li^7(\alpha, \alpha')H^3He^4$ ($Q = -2.465$ Mev). The large peak at a lower pulse height than the 4.61-Mev peak is due to alpha particles scattered from hydrogen.

B. Angular Distributions

1. Inelastic Scattering

a. Li^7 ($\epsilon = 4.61$ Mev)

The angular distributions obtained for the 4.61-Mev level of Li^7 by proton and alpha-particle bombardments are shown in Figs. 9 and 10. The errors are the standard deviations for the relative cross sections only. The gap in the data at the peak of the first maximum in the alpha-particle distribution is a consequence of the hydrogen contamination. Alpha particles incident on the hydrogen scatter only into angles less than 14.6° in the laboratory system, and consist of two energy groups for each angle. The higher-energy group moved across the 4.61-Mev peak at angles between 8° and 11° and was approximately 50% larger than the 4.61-Mev peak. Attempts to subtract off the hydrogen contribution were made, using published data, but the uncertainties in the normalization to the published data made the results unreliable.

These data were fitted with the direct-interaction theory of ABM. Neglecting all interactions with the nuclear core and assuming that the incident particle interacts only with a single nucleon at the surface of the nucleus, one finds for the differential cross section the angular dependence

$$\frac{d\sigma}{d\Omega} \sim \left[j_{\ell}(ga)\right]^2 ,$$

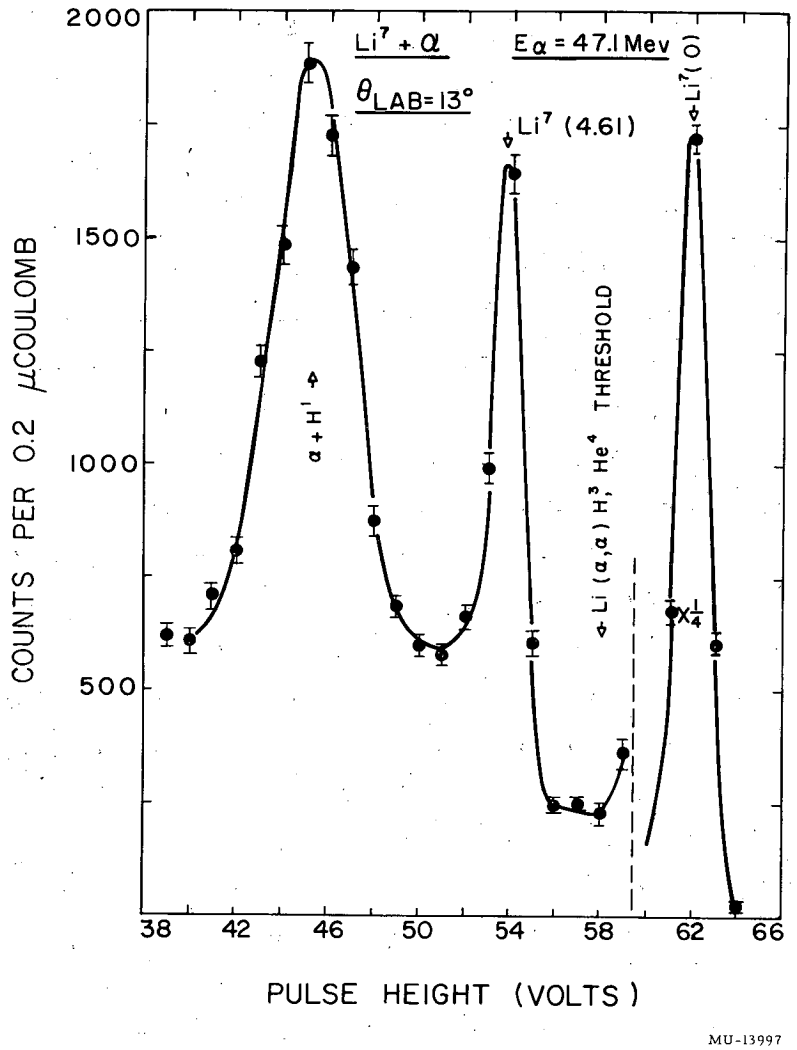

Fig. 8. Sodium iodide spectrum for 13° in the alpha-particle experiment, showing the effect of hydrogen in the target.

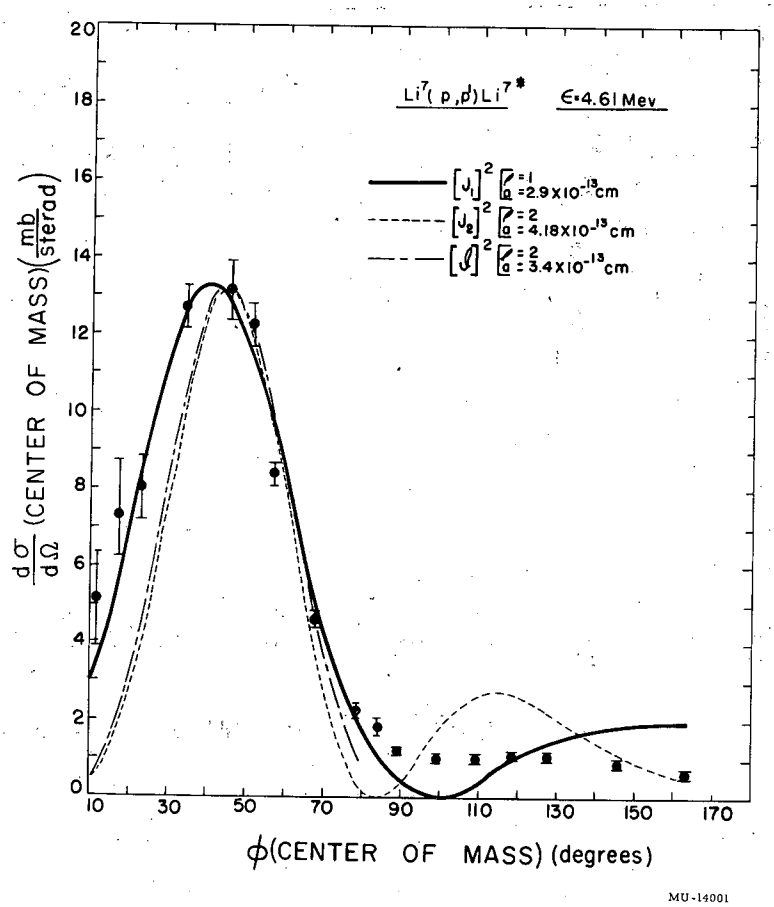

Fig. 9. Differential cross section for $Li^7(p, p')Li^{7*}$ (ϵ = 4.61 Mev) at 31.8 Mev incident energy.

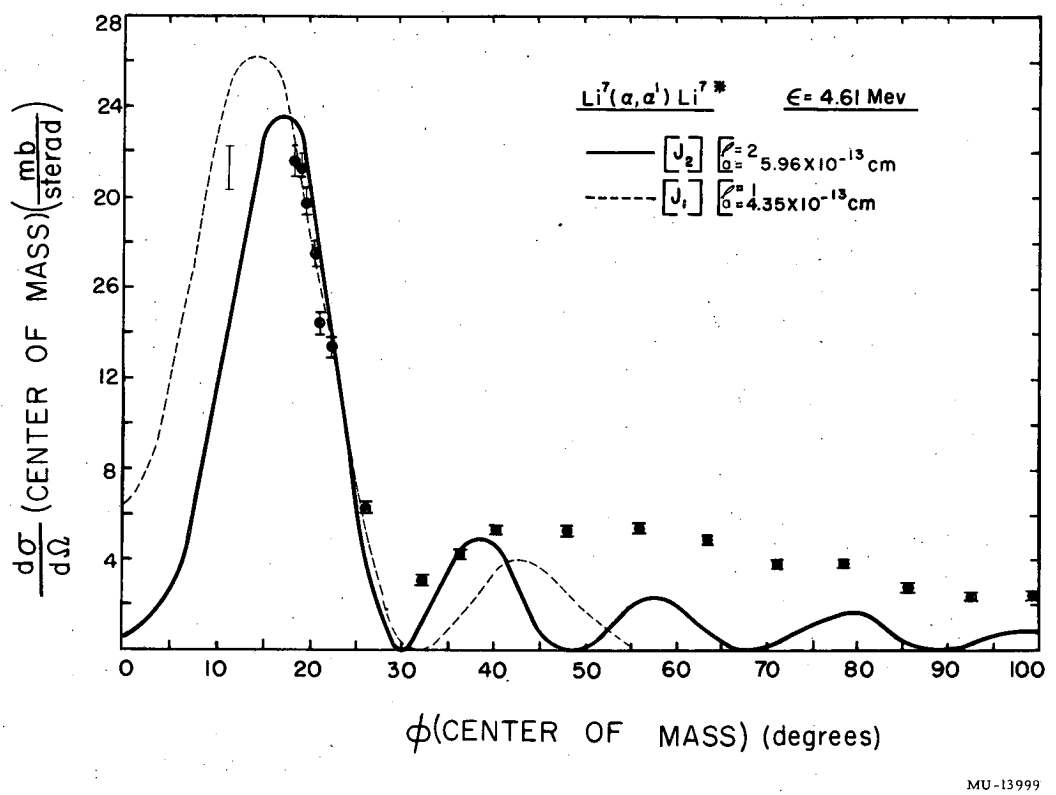

Fig. 10. Differential cross section for $Li^7(\alpha, \alpha')\ Li^{7*}$ (ϵ = 4.61 Mev) at 47.1 Mev incident energy.

where $g = \left|\vec{k}_i - \vec{k}_f\right|$

$\vec{k}_i$ is the propagation vector of the incident particle,

$\vec{k}_f$ is the propagation vector of the outgoing particle,

a is the radius at which the interaction is assumed to take place,

ℓ is the orbital angular momentum imparted to the nucleus in the collision, and

j_ℓ is the spherical Bessel function of order ℓ.

The radius a is used as a variable parameter in the fitting of the data. The selection rules for the spin and parity are

$$J_i + J_f \geq \ell \geq \left|\vec{J}_i + \vec{J}_f\right|_{min}$$

and

$$\pi_f = (-1)^\ell \pi_i ,$$

where there is no spin change between the incident and outgoing particles. J_i and J_f are the spins of the initial and final nuclear states, respectively. This applies to alpha-particle scattering. For proton scattering, including the possibility of spin flip,

$$J_i + J_f + 1 \geq \ell \geq \left|\vec{J}_i + \vec{J}_f + \vec{1}\right|_{min}$$

and

$$\pi_f = (-1)^\ell \pi_i$$

The ℓ value obtained by fitting j_ℓ^2 to the first maximum of the data is the minimum value consistent with the above selection rules.

The proton data for the 4.61-Mev level were best fitted with $\ell = 1$ and $a = 2.9 \times 10^{-13}$cm ($1.52A^{1/3} \times 10^{-13}$cm). Since the ground state of Li^7 is a $3/2^-$ state, this implies even parity for the 4.61-Mev level and $J = 1/2^+$, $3/2^+$, $5/2^+$, or $7/2^+$. The curve for $\ell = 2$ is also shown in Fig. 9. It does not give so good a fit to the first maximum, and the radius, $a = 4.18 \times 10^{-13}$cm($2.19A^{1/3} \times 10^{-13}$cm), is large.

In the derivation of the expression for the angular distribution given above, the interaction was assumed to take place at a radius $r = a$, and contributions from the nucleon wave function for $r > a$ were ignored. (See Appendix A.) The calculations were extended to $r \geq a$ for $\ell = 2$, and the results are plotted in Fig. 9 as $[\mathcal{J}]^2$. They show a slight broadening of the first maximum without much improvement in the fit, although the minimum radius required is now a more reasonable number 3.4×10^{-13} cm or $1.78A^{1/3} \times 10^{-13}$ cm.

A unique fit to the alpha-particle data for the 4.61-Mev level was not possible. Curves for $\ell = 1$ and $\ell = 2$ using reasonable radii for alpha-particle scattering are shown in Fig. 10. Either curve must be

considered as a possible fit. If $\ell = 1$ were correct the spin and parity of the 4.61-Mev level would be $1/2^+$, $3/2^+$, or $5/2^+$. For $\ell = 2$ it would be $1/2^-$, $5/2^-$, or $7/2^-$. $J = 3/2^-$ could be formed by a zero transfer of angular momentum ($\ell = 0$), which means that a fit with j_o^2 should be possible. The data do not indicate a peak at 0°, which this would require. If one were to ignore the point at 11^o(c.m.) and fit j_o^2 to the remaining data, the required radius, $a = 3.24 \times 10^{-13}$cm, would be small compared with the usual values needed for fitting alpha-particle data.

The evidence from other experiments does not establish the spin and parity for this level. Erdos et al.[30] suggest the values $J = 5/2^-$ or $3/2^-$ on the basis of the angular distribution of tritons from the reaction $Li^7(\gamma, t)He^4$. Levine et al.[31] were not able to fit any present theory to their angular distribution of inelastically scattered deuterons. Haffner[32] examined the same reaction at $E_d = 15$ Mev (0.5 Mev higher than in the experiment by Levine et al., and fit the forward peak to j_1^2. This implies $J = 1/2^+$, $3/2^+$, or $5/2^+$, in agreement with the proton results described in this paper. The angular distributions obtained by Conzett for the inelastic scattering of 12-Mev protons suggest $J = 5/2^-$ or $3/2^-$, but do not exclude the possibility of $7/2^-$.[12] The latter is what one would expect on the basis of the intermediate coupling model if the 4.61-Mev level is the lower-energy component from the splitting of the ^2F state.[33] The other half of the split pair, with a J of $5/2^-$ could correspond to the 7.46-Mev level, for which $5/2^-$ has been obtained experimentally.[17]

In the experiment described here the good fit for $\ell = 1$ in the proton data may be misleading. The use of j_ℓ^2 or $\mathcal{J}^2$ implies that the nucleus can be represented as opaque to the incident particle. While this may be a good representation when an alpha particle is either the incident or outgoing particle, it may not hold for protons, particularly in light nuclei.[34] Some idea of the degree of transparency of the Li^7 nucleus to protons of 31.5 Mev may be obtained from the optical-model parameters used by Melkanoff et al.[35] to fit the elastic data of Kinsey and Stone.[29] Using $\lambda \approx \frac{\hbar\sqrt{E + V}}{W\, 2m}$ for the mean free path, where E

is the energy of the proton in the c.m. (28 Mev), V is the real part of the potential well (44 Mev), W is the imaginary part (11 Mev), and M is the reduced mass, one obtains a value of 3.5×10^{-13} cm. The radius of the lithium nucleus calculated from $R = 1.28 A^{1/3} \times 10^{-13}$ cm is 2.5×10^{-13} cm. Here λ is seen to be on the order of R, implying that contributions from the core to the direct-interaction process cannot be ignored.

It would be desirable to extend these calculations to include the core effects as a check on the $\ell = 1$ fit. The reaction $Li^6(d, p)Li^7$ could also give valuable information on the parity of the 4.61-Mev level. Such an experiment is planned for the near future.

b. $Li^7(\epsilon = 6.6$ Mev)

Data for the 6.6-Mev level were taken in the proton bombardments only. The angular distribution is shown in Fig. 11. The best fit to the data was obtained for $\ell = 1$ and $a = 3.37 \times 10^{-13}$ cm ($1.76 A^{1/3} \times 10^{-13}$ cm); $\ell = 2$ was also tried, but the fit to the first maximum was not good. It also required a radius of $a = 5.4 \times 10^{-13}$ cm ($2.82 A^{1/3} \times 10^{-13}$ cm), which is too large to be acceptable. The $\ell = 1$ fit implies a change in parity between the ground state and the 6.6-Mev level, and permits the values $1/2^+$, $3/2^+$, $5/2^+$, or $7/2^+$ for the spin and parity of this state.

Other evidence on which the spin and parity of this level can be based is sketchy. The large thermal-neutron-capture cross section in Li^6 (Q = 7.245 Mev) could be due to the presence of this level.[17] The formation of the level by S-wave neutrons along with a J of 1^+ for the Li^6 ground state would give $1/2^+$ or $3/2^+$ for the spin and parity of the 6.6-Mev level. Erdos et al.[30] see this level with the reaction $Li^7(\gamma, t)He^4$, and from the angular distribution of tritons they suggest $J = 5/2^-$, $3/2^-$, or $1/2^-$, with some possibility for $1/2^+$. The only agreement between these data is for the assignment $1/2^+$ to the 6.6-Mev level; however, the evidence is not conclusive enough to draw a final inference.

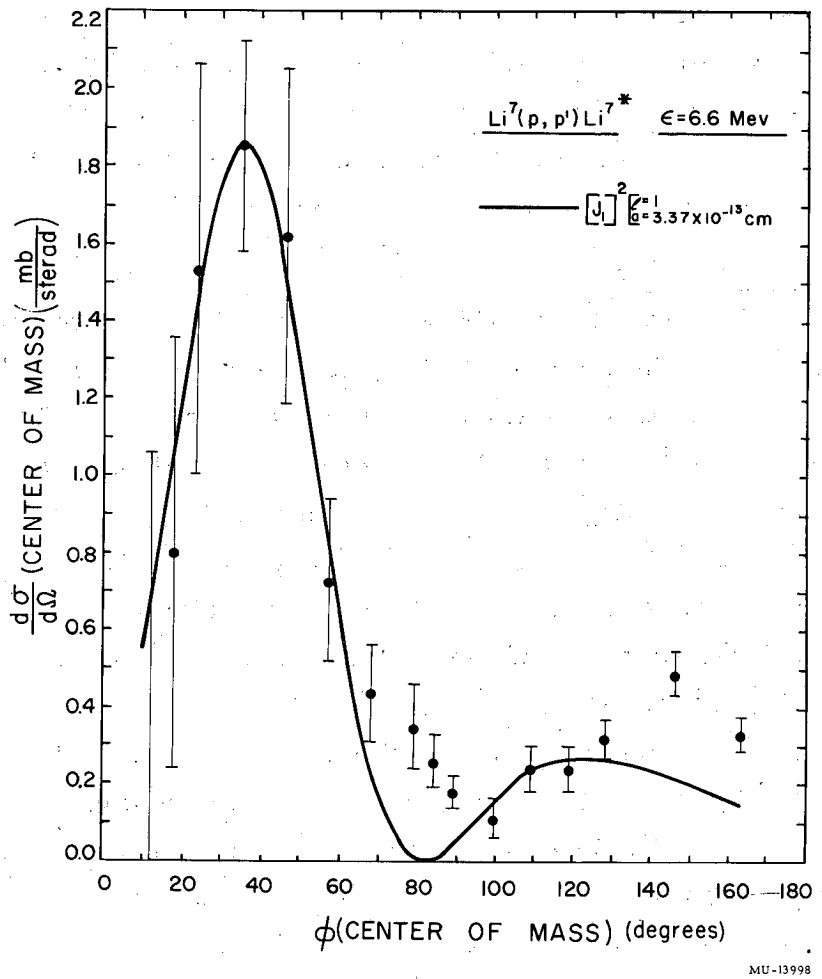

Fig. 11. Differential cross section for $Li^7(p, p')Li^{7*}$ (ϵ = 6.6 Mev).

c. $Li^6(\epsilon = 0$ and 2.19 Mev)

The angular distributions obtained for the $Li^7(p,d)Li^6$ reaction leading to the ground state and 2.19-Mev level of Li^6 are plotted in Figs. 12 and 13. The inverse Butler stripping theory was used to fit the data.[5,18] (See Appendix B.) The section rules are

$$J_f + J_i + 1/2 \geq \ell_n \geq \left| \vec{J}_f + \vec{J}_i + \vec{1/2} \right|_{min}$$

and

$$\pi_f = (-1)^{\ell_n} \pi_i ,$$

including the change in spin of 1/2 between the incident proton and outgoing deuteron. The proton spin is assumed not to have flipped in picking up the neutron. The ℓ_n value needed to fit the first maximum of the experimental data corresponds to the minimum value consistent with the above selection rules.

Both distributions were best fitted when the picked up neutron was assumed to carry off one unit of orbital angular momentum ($\ell_n = 1$). This required a radius of 4.2×10^{-13} cm for the ground state and 4.5×10^{-13} cm for the 2.19-Mev level. Additional calculations were made for $\ell_n = 0$ and $\ell_n = 2$. The $\ell_n = 0$ curves did not fit the data for either level (shown only for $\epsilon = 0$, though the results are similar for the 2.19-Mev level). Fits could be made with $\ell_n = 2$, but the a values required were too large.

The possible spin and parity values for $\ell_n = 1$ and $J_i(Li^7) = 3/2^-$ are $J_f = 0^+, 1^+, 2^+$, or 3^+. The ground state of Li^6 has been measured as 1^+ and the 2.19-Mev level as 3^+.[17] The results presented here are consistent with these assignments.

Reynolds and Standing[36] obtained angular distributions for the same reactions at $E_p = 18$ Mev. Their results were also fitted with $\ell_n = 1$. The radius required was 5.5×10^{-13} cm for both distributions.

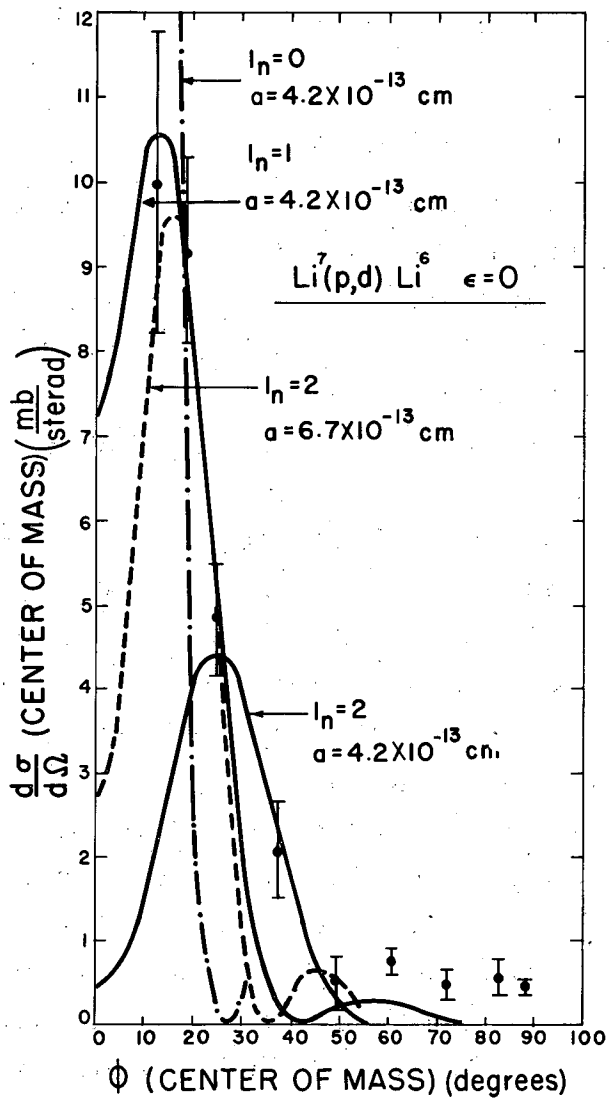

Fig. 12. Differential cross section for the pickup reaction $Li^7(p,d)Li^6$, to the ground state of Li^6.

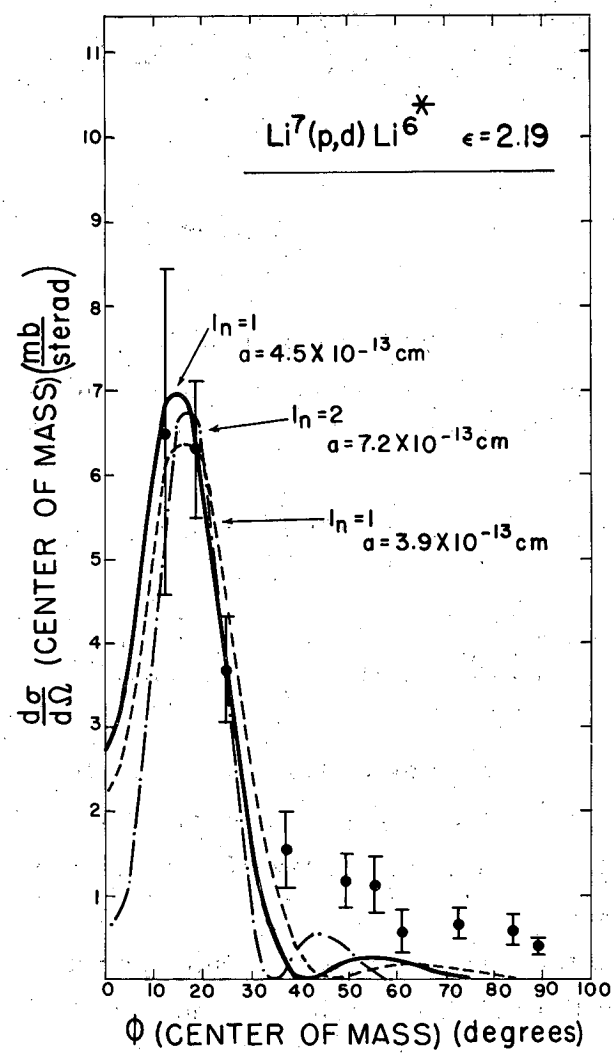

Fig. 13. Differential cross section for the pickup reaction $Li^7(p,d)Li^6$ to the 2.19-Mev level of Li^6.

APPENDIX

A. Direct-Interaction Theory

The direct-interaction theory of ABM including the region $r \geq a$ results in an angular dependence for the differential cross section of the form[5]

$$\frac{d\sigma}{d\Omega} \sim \left[\mathcal{J}\right]^2 = \left[\int_a^\infty h_{\ell_n}(i k_{os} r_n) h_{\ell_{n'}}(i k_{ts} r_n) j_\ell(g a) dr_n\right]^2 ,$$

where

$$g = \left| \vec{k}_i - \vec{k}_f \right| ,$$

$\vec{k}_i$ is the propagation vector of the incident particle,

$\vec{k}_f$ is the propagation vector of the outgoing particle,

ℓ_n is the orbital angular momentum of the nucleon in the initial nucleus,

$\ell_{n'}$ is the orbital angular momentum of the nucleon in the final state,

$$k_{os} = \frac{\sqrt{2 M_n B_{os}}}{\hbar} \quad \text{and} \quad k_{ts} = \frac{\sqrt{2 M_n B_{ts}}}{\hbar} ,$$

B_{os} is the binding energy of the nucleon to the remainder of the nucleus (core in state s) before excitation,

B_{ts} is the binding energy of the nucleon in the excited state (core in state s),

j_ℓ is the spherical Bessel function of order ℓ,

ℓ is the orbital angular momentum imparted to the nucleus in the collision,

h_{ℓ_n}, $h_{\ell_{n'}}$ are spherical Hankel functions of order ℓ_n and $\ell_{n'}$ respectively (they represent the external wave functions of the bound nucleon that interacts with the incident particle), and

a is the minimum radius at which the direct interaction is assumed to take place.

This formulation assumes that the interaction takes place through single-particle excitation, and neglects Coulomb effects.

The angular dependence in the differential cross section is contained entirely in the term $j_\ell(g\,a)$. If the reaction is assumed to take place only at $r = a$, the (relative) differential cross section is seen to reduce to $\left[j_\ell \right]^2$.

For the $Li^7(p, p')\,Li^{7*}$ (ϵ = 4.61 Mev) calculation, ℓ_n and $\ell_{n'}$ were taken equal to unity on the basis of the intermediate coupling model.[33] The ground state and 4.61-Mev level represent different configurations of the nucleons in the p shell. The binding energies were taken as 10 Mev and 5.4 Mev. These represent an average for the possible core states rather than the binding energy of the least tightly bound nucleon.

For $\ell_n = \ell_{n'} = 1$, $\left[\mathcal{J}\right]^2$ can be written

$$\left[\mathcal{J}\right]^2 = \left\{ \int_{\rho o}^{\infty} \frac{e^{-(1+\alpha)\rho}}{\alpha\, k_{os}^{3}} \left[1 + \left(\frac{1}{\alpha} + \frac{1}{\alpha^2}\right) \frac{1}{\rho} + \frac{1}{\alpha^2 \rho^2} \right] j_\ell \left(\frac{g}{k_{os}} \rho \right) d\rho \right\}^2 ,$$

where

$$\rho = k_{os} r_n \quad \text{and} \quad \alpha = \frac{k_{ts}}{k_{os}} .$$

The integration was performed numerically.

B. Inverse Butler Stripping

The differential cross section for the inverse Butler stripping reaction can be written

$$\frac{d\sigma}{d\Omega} \sim \left[\frac{1}{k^2+a^2} - \frac{1}{k^2+(a+b)^2}\right]^2 \left\{ A_{\ell_n} j_{\ell_n}(ga) + B_{\ell_n} \left(\frac{ga}{2\ell_n+1}\right) \right.$$

$$\left. \times \left[\ell_n j_{\ell_n}(ga) - (\ell_n+1)\, j_{\ell_n+1}(ga)\right]\right\}^2 ,$$

where

$$k = \left| \frac{1}{2} \vec{k}_d - \vec{k}_p \right| ,$$

$$g = \left| \vec{k}_d - \vec{k}_p \right| ,$$

a is the interaction radius,

$$\left.\begin{array}{l} a = 2.32 \times 10^{12} \mathrm{cm}^{-1} \\ b \simeq 6\, a \end{array}\right\} \text{are constants of the deuteron wave function,}$$

$$A_{\ell_n} = \sum_{r=0}^{\ell_n} \frac{(\ell_n + r)!\ (k_s a + r + 1)}{r!\ (\ell_n - r)!\ (2k_s a)^r} ,$$

$$B_{\ell_n} = \sum_{r=0}^{\ell_n} \frac{(\ell_n + r)!}{r!\ (\ell_n - r)!\ (2k_s a)^r} ,$$

$$i k_s = k_n = \frac{\sqrt{2m_n E_n}}{\hbar} , \quad E_n = E_d - \epsilon_d - E_p ,$$

ϵ_d is the binding energy of the deuteron,

ℓ_n is the orbital angular momentum carried by the picked up neutron, and

E_d and E_p are the c.m. energies of the deuteron and proton respectively.

ACKNOWLEDGMENTS

The author wishes to acknowledge his indebtedness as follows:

To Professor Luis W. Alvarez for his interest and encouragement.

To Dr. Homer E. Conzett for his active participation in all phases of the alpha-particle experiment.

To Mr. H. Paul Huish for his considerable help during the proton runs.

To Dr. H.B. Knowles, Dr. George J. Hecht, and Dr. John Leahy for assistance during the proton runs; and to Dr. Rodolfo Slobodrian, Mr. Harlan Shaw, and Mr. Dennis Hoffman for assistance during the alpha particle runs.

To Dr. Warren Heckrotte, Dr. Homer E. Conzett, Dr. H.B. Knowles, and Dr. George J. Hecht for many helpful and stimulating discussions.

The author also wishes to acknowledge the skill and cooperation of the linear accelerator crew, the cyclotron crew, and the electronics maintenance crew, especially Mr. William Gantz, Mr. George Constantian, and Mr. Fred Vogelsberg.

This work was done under the auspices of the United States Atomic Energy Commission.

REFERENCES

1. Statistical Aspects of the Nucleus, Brookhaven National Laboratory, BNL-331 (C-21), Jan. 1955.
2. N. Bohr, Nature 137, 344 (1936).
3. J.M. Blatt and V.F. Weisskopf, Theoretical Nuclear Physics (Wiley, New York, 1952).
4. Austern, Butler, and McManus, Phys. Rev. 92, 350 (1953).
5. S.T. Butler, Phys. Rev. 106, 272 (1957).
6. See S.T. Butler, op. cit, for a semiclassical argument on this point.
7. G.E. Fischer, Phys. Rev. 96, 704 (1954);
   The Scattering of 10-Mev Protons on Carbon and Magnesium (Thesis), UCRL-2546, Apr. 1954).
8. R.G. Summers-Gill, Some Properties of the Beryllium Nucleus Obtained from Scattering Data (Thesis), UCRL-3388 Apr. 1956.
9. F.J. Vaughn, Elastic and Inelastic Scattering of 48-Mev Alpha Particles by Carbon and Magnesium (Thesis), UCRL-3174, Oct. 1955.
10. Benveniste, Finke, and Martinelli, Phys. Rev. 101, 655 (1956).
11. G.J. Hecht, Angular Distributions of Charged Particles from 31-Mev Protons on Carbon (Thesis), UCRL-2969, Apr. 1955.
12. H.E. Conzett, Phys. Rev. 105, 1324 (1957).
13. P.C. Gugelot and P.R. Phillips, Phys. Rev. 101, 1614 (1956).
14. P.C. Gugelot and M. Rickey, Phys. Rev. 101, 1613 (1956).
15. A. Bohr and B.R. Mottelson Kgl. Danske Videnskah. Selskap Mat.-fys. Medd. 29, No. 16 (1953).
16. S. Hayakawa and S. Yoshida, Proc. Phys. Soc. (London) 68A, 656 (1955);
    Prog. Theo. Phys. (Japan) 14, 1 (1955).
17. T. Ajzenberg and T. Lauritsen, Revs. Modern Phys. 27, 77 (1955).
18. S.T. Butler, Proc. Roy. Soc. (London) A208, 559 (1951).
19. R. Huby, Stripping Reactions, in Progress in Nuclear Physics O.R. Frisch, Ed. (Pergamon Press, London, 1953). Chap. 7

20. W. Tobocman and M.H. Kalos, Phys. Rev. 97, 132 (1955).

21. L.W. Alvarez and many others, Rev. Sci. Instr. 26, No. 2, 111 (1955).

22. R. Mather and E. Segrè, Phys. Rev. 84, 191 (1951).

23. Aron, Hoffman, and Williams, Range-Energy Curves, AECU-663 (Rev.), 1949.

24. H.R. Bowman and R.E. Thomas, Multichannel Pulse-Height Analyzer UCRL-2164, Apr. 1953

25. R.E. Ellis, Elastic Scattering of 48-Mev Alpha Particles by Heavy Nuclei (Thesis), UCRL-3114, Aug. 1955.

26. Taylor, Jentschke, Remley, Eby, and Kruger, Phys. Rev. 84, 1034 (1951).

27. S.K. Allison and H. Casson, Phys. Rev. 90, 880 (1953).

28. J.B. Berks, Scintillation Counters (McGraw-Hill, New York, 1953).

29. B.B. Kinsey and T. Stone, Phys. Rev. 103, 975 (1956).

30. P. Erdös , P. Stoll, and M. Wächter, Nuovo cimento 12, 639 (1954).

31. Levine, Bender, and McGruer, Phys. Rev. 97, 1249 (1955).

32. J.W. Hoffner, Phys. Rev. 103, 1398 (1956).

33. D.R. Inglis, Revs. Modern Phys. 25, 390 (1953);
D. Kurath, Phys. Rev. 101, 216 (1956).

34. Compare results of References 8 and 10 for Be^9 (ϵ = 2.43);
References 9 and 11 for C^{12} (ϵ = 4.43);
References 13 and 14 for Mg^{24} (ϵ = 1.37).

35. Melkanoff, Nodvik, Saxon, and Woods, Phys. Rev. 106, 793 (1957).

36. J.B. Reynolds and K.G. Standing, Phys. Rev. 101, 158 (1956).